

Crosstalk measurements from PAPER-64

Saul A. Kohn* & James E. Aguirre

University of Pennsylvania

August 8, 2015

Abstract

Crosstalk is artificial signal created by an interferometer that contaminates the astronomical visibilities it is built to measure. We present extremely compelling evidence that the dominant source of crosstalk for PAPER-64 is reflections between antenna pairs, demonstrating a $1/R^2$ dependence for antenna-separation R . Some crosstalk is seen in excess of this trend, and may be due to crosstalk between dipole arms on individual antennae. Natural extensions of this work are a full modelling of reflections throughout the array, a visibility-based analysis of leakage between dipole arms, and a more complete treatment of polarization calibration.

1 Introduction & Theory

Cross-talk is an effect in which signals from one antenna are picked up by an adjacent antenna, causing an erroneous correlation. This effect is important at low frequencies in compact configurations. In this memo, we describe measurements of crosstalk in data from the PAPER-64 EoR observation season. We quantify the effect of total crosstalk on PAPER's standard measurements, which we will show is largely dependent on the antenna configuration.

In this section, we introduce a mathematical model of crosstalk. We outline our measurement techniques in Section 2, and present our measurements in Section 3. We discuss the implications of our results and conclude in Section 4.

1.1 Dipole-arm crosstalk

Crosstalk between dipole arms on a given antenna m can be described by (neglecting noise terms):

$$\begin{aligned} X'_m &= X_m + D_m^x Y_m \\ Y'_m &= Y_m + D_m^y X_m \end{aligned}$$

So an observed XX visibility becomes contaminated by noise-like XY and YX visibilities:

$$X'_m X'_n = X_m X_n + D_m^x Y_m X_n + D_n^x X_m Y_n + \mathcal{O}(D^2) \quad (1)$$

Which is negligible compared to the XX signal. However, this *polarized leakage* is symmetric, causing XX and YY to leak into XY :

$$X'_m Y'_n = X_m Y_n + D_m^x Y_m Y_n + D_n^y X_n X_m + \mathcal{O}(D^2) \quad (2)$$

This demonstrates the importance of trying to remove crosstalk when making measurements of polarization – the cross-polarizations will be completely overpowered by the XX and YY terms otherwise.

1.2 Reflection crosstalk

We can describe crosstalk from reflections between antenna pair (m, n) as:

$$X'_m = X_m + \epsilon_{mn}^x X_n + \epsilon_{mn}^y Y_n; \quad \epsilon_{mn}^p \propto \frac{1}{|m-n|^2} \quad (3)$$

with a similar definition for Y_m ; $|m-n|$ represents the physical distance between antennae m and n . This means that the observed XX visibility between antennae becomes:

$$X'_m X'_n = X_m X_n + \epsilon_{nm}^x X_m X_m + \epsilon_{mn}^x X_n X_n + \epsilon_{nm}^y X_m Y_m + \epsilon_{mn}^y Y_n X_n + \mathcal{O}(\epsilon^2) \quad (4)$$

However the XY visibilities are noise-like, so effectively:

$$X'_m Y'_n \approx X_m Y_n + \epsilon_{nm}^x X_m X_m + \epsilon_{mn}^x X_n X_n \quad (5)$$

Implying that the observed XX visibilities are contaminated by over-the-air crosstalk from autocorrelations of nearby antennae.

*saulkohn@sas.upenn.edu

1.3 Putting it together

Using these models, we can represent crosstalk on a given dipole arm as:

$$\begin{pmatrix} X'_m \\ Y'_m \end{pmatrix} = \begin{pmatrix} 1 & D_m^x \\ D_m^y & 1 \end{pmatrix} \begin{pmatrix} X_m \\ Y_m \end{pmatrix} + \begin{pmatrix} \epsilon_{mn}^{xx} & \epsilon_{mn}^{xy} \\ \epsilon_{mn}^{yx} & \epsilon_{mn}^{yy} \end{pmatrix} \begin{pmatrix} X_n \\ Y_n \end{pmatrix} \quad (6)$$

We can represent this in a more condensed form as:

$$\vec{m}' = \mathbf{D}_m \vec{m} + \mathbf{E}_{mn} \vec{n} \quad (7)$$

Such that:

$$\vec{m}' \otimes \vec{n}' = \begin{pmatrix} X_m X_n & X_m Y_n \\ Y_m X_n & Y_m Y_n \end{pmatrix} = (\mathbf{D}_m \vec{m} \otimes \mathbf{D}_n \vec{n}) + (\mathbf{D}_m \vec{m} \otimes \mathbf{E}_{nm} \vec{m}) + (\mathbf{E}_{mn} \vec{n} \otimes \mathbf{D}_n \vec{n}) + (\mathbf{E}_{mn} \vec{n} \otimes \mathbf{E}_{nm} \vec{m}) \quad (8)$$

Neglecting terms $\mathcal{O}(D^2)$, $\mathcal{O}(\epsilon^2)$ and $\mathcal{O}(D\epsilon)$, these outer products reduce as expected:

$$\mathbf{D}_m \vec{m} \otimes \mathbf{D}_n \vec{n} \approx \begin{pmatrix} X_m X_n + D_m^x Y_m X_n + D_n^x X_m Y_n & X_m Y_n + D_m^x Y_m Y_n + D_n^y X_m X_n \\ Y_m X_n + D_n^x Y_m Y_n + D_m^y X_m X_n & Y_m Y_n + D_n^y Y_m X_n + D_m^y X_m Y_n \end{pmatrix} \quad (9)$$

$$\mathbf{D}_m \vec{m} \otimes \mathbf{E}_{nm} \vec{m} \approx \begin{pmatrix} \epsilon_{nm}^{xx} X_m X_m + \epsilon_{nm}^{xy} X_m Y_m & \epsilon_{nm}^{yx} X_m X_m + \epsilon_{nm}^{yy} X_m Y_m \\ \epsilon_{nm}^{xx} Y_m X_m + \epsilon_{nm}^{xy} Y_m Y_m & \epsilon_{nm}^{yx} Y_m X_m + \epsilon_{nm}^{yy} Y_m Y_m \end{pmatrix} \quad (10)$$

$$\mathbf{E}_{mn} \vec{n} \otimes \mathbf{D}_n \vec{n} \approx \begin{pmatrix} \epsilon_{mn}^{xx} X_n X_n + \epsilon_{mn}^{xy} Y_n X_n & \epsilon_{mn}^{xx} X_n Y_n + \epsilon_{mn}^{xy} Y_n Y_n \\ \epsilon_{mn}^{yx} X_n X_n + \epsilon_{mn}^{yy} Y_n X_n & \epsilon_{mn}^{yx} X_n Y_n + \epsilon_{mn}^{yy} Y_n Y_n \end{pmatrix} \quad (11)$$

and all elements of $\mathbf{E}_{mn} \vec{n} \otimes \mathbf{E}_{nm} \vec{m}$ are negligible, such that:

$$X'_m X'_n \approx X_m X_n + D_m^x Y_m X_n + D_n^x X_m Y_n + \epsilon_{nm}^{xx} X_m X_m + \epsilon_{nm}^{xy} X_m Y_m + \epsilon_{mn}^{xx} X_n X_n + \epsilon_{mn}^{xy} Y_n X_n \quad (12)$$

i.e. neglecting crosstalk coupled with the much weaker XY and YX visibilities, we recover the sum of Equations 4 and 1.

2 Method

2.1 Measuring total crosstalk

We model total crosstalk as if it is constant over time. As shown above, this is not quite true, since the amount of reflection crosstalk is proportional to the autocorrelations, and these in turn are proportional to sky temperature. However, a constant over time is usually a good approximation, especially for the large amount of the season in which the Galaxy is not transiting zenith during observations.

Using this constant-over-time model, we proceed with a number of steps to constrain the crosstalk signal based on time-averaged visibilities, extracting the average:

- visibility for each baseline, over a 10 minute observation
- visibility for each baseline, over a night of observations
- visibility for each baseline type over a night of observations

where ‘‘baseline type’’ refers to a given antenna separation within the PAPER-64 grid. In this case, crosstalk removal is simply a subtraction of the nightly average for each baseline. For analysis of reflection crosstalk we focus on fiducial night JD2456250 from early in the PAPER-64 season, analysing the visibilities between LST=0–8 hours. It has been roughly calibrated to a common Jy scale, allowing for comparisons between baselines. This night has comparable crosstalk levels to other nights in the season, and presents small deviations ($< 3\sigma$) from the median sky model at the central frequency of 145 MHz. The effect of total crosstalk subtraction on a fiducial 30 m baseline is shown in Figure 1.

2.2 Measuring dipole-arm crosstalk

The leakage between dipole arms is not configuration dependent. Under the assumption of identical feeds, one can proceed to solve for D-terms using an image-based method with Stokes I , Q , U and V . This measurement involves a more complete treatment of Jones matrices, parallactic angle rotation of bright sources and widefield beam effects, and will be presented in its own memo (Nunhokee et al. HERA memo in prep).

2.3 Measuring individual reflections

Measuring reflections independent of total crosstalk is a difficult endeavour, outside the scope of this memo. Since the ϵ_{ij}^{pq} values are coupled to autocorrelations throughout the array, one needs to model each dipole ‘broadcasting’ a fraction of its autocorrelation to every other antenna. If we consider the case of no D-term leakage, as written in Equation 4, we see that even in the limit of autocorrelations being unaffected by crosstalk (i.e. $X'_m X'_m = X_m X_m$) there are still 3 unknown parameters per visibility: the ‘true’ visibility $X_m X_n$, ϵ_{mn}^{xx} and ϵ_{mn}^{xy} . This crosstalk will technically vary on the timescale of a single autocorrelation, so it is difficult to argue for a least-squares technique, which assumes couplings that are constant in time.

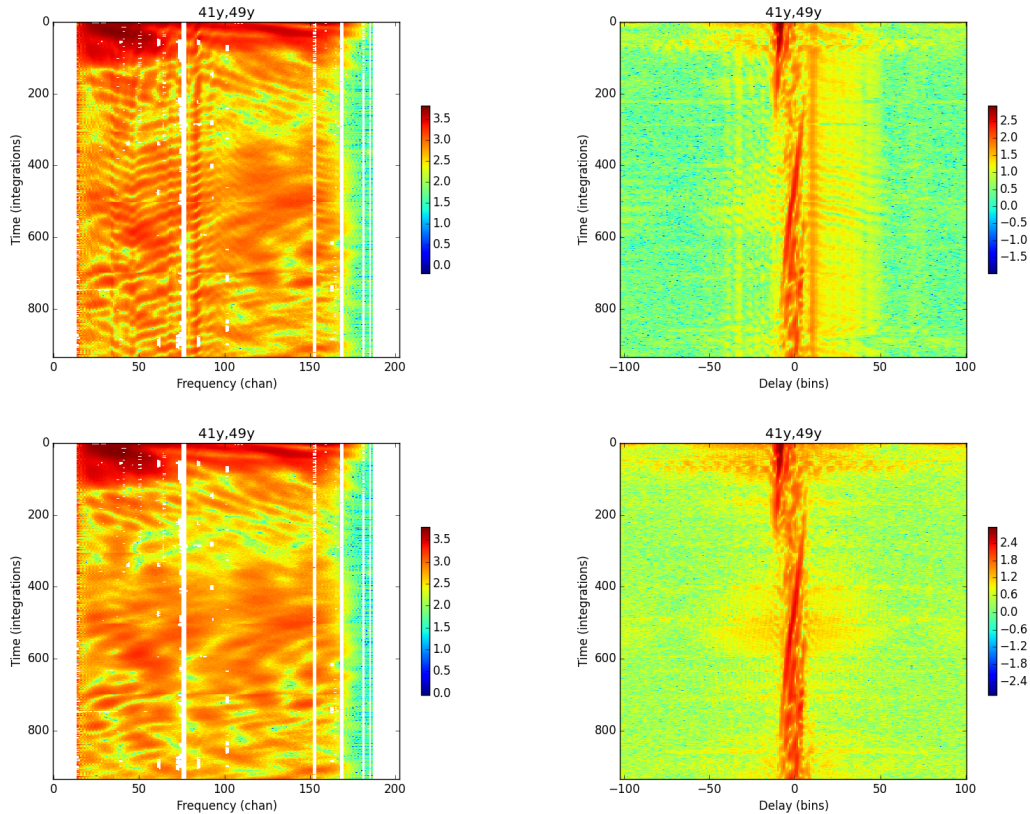


Figure 1: *Top*: Waterfall plots of the real part of YY visibilities on a 30 m baseline in frequency- (left) and delay-space (right). Note the constant-in-time signal on the horizon at positive delay. *Bottom*: the same as above, but after crosstalk subtraction. The bright excess at integration numbers <200 is solar. These visibilities have not been CLEANed, leading to noticeable leakage outside of the horizon in delay space.

3 Results

3.1 Total crosstalk

In Figure 2, we show the average visibility on a fiducial 30 m baseline for each 10 minute integration (left) and the total average (right) over JD2456250. Close to the start of the observation season, the Galaxy is not present in this data. Sunset can be seen, with much larger average visibilities at the start of the night (top; note that the sun is technically below the horizon at this time). The dip at 137 MHz is the always-flagged ORBCOMM satellite band. The flat lines on both ends of the spectrum are the always-flagged band edges. Note that the total crosstalk in any given integration appears to be roughly constant, but that it does change in profile throughout the night. This data has already been RFI-flagged twice, once in high and once in low spectral resolution.

3.2 Reflections

Consider a plane wave incident on antenna m , which reflects onto antenna n . Such a reflected signal would have a delay corresponding to the distance between the antennae. We can investigate the presence of such reflections by delay-transforming the average visibilities of different baseline-types and looking for resonances at the corresponding delays. An example of this method is shown in Figure 3, which shows the night-averaged visibilities on all of the 30 m baselines in the array (left) and the median of those signals (right). In both plots, there is a clear resonance exactly at the delay corresponding to the 30 m baseline length in both directions, suggesting that reflections are dominating the crosstalk signal.

We make a further test of the hypothesis that the dominant source of crosstalk is reflections by measuring the average crosstalk on each baseline type (30, 60, 90 and 120 m baselines). These are shown in Figure 4; indeed, we see the maximum signal in delay-space (which always lines-up with baseline separation delays) decrease by approximately a factor of 4 for each increase in spacing, i.e. a $1/R^2$ dependence.

It is important to understand the magnitude of crosstalk compared to typical visibilities. This is a little difficult to communicate effectively, since we have measured crosstalk under the definition of a time-average over the visibilities. However, if define a parameter ξ_V :

$$\xi_V = \frac{1}{T} \sum_t \frac{V(\nu)}{\sqrt{\sum_\nu |V(\nu)|^2}} \quad (13)$$

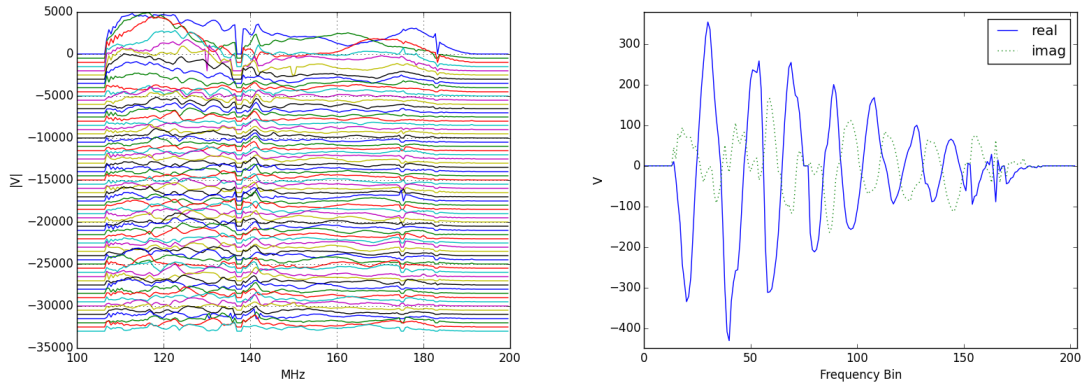


Figure 2: *Left*: The average YY (absolute-value) visibility for a single 30 m baseline of each 10 minute file over the night, plus a constant offset for display purposes. The average of the first file is at the top, and file time progresses downwards. *Right*: The time-averaged visibility for that baseline over the night.

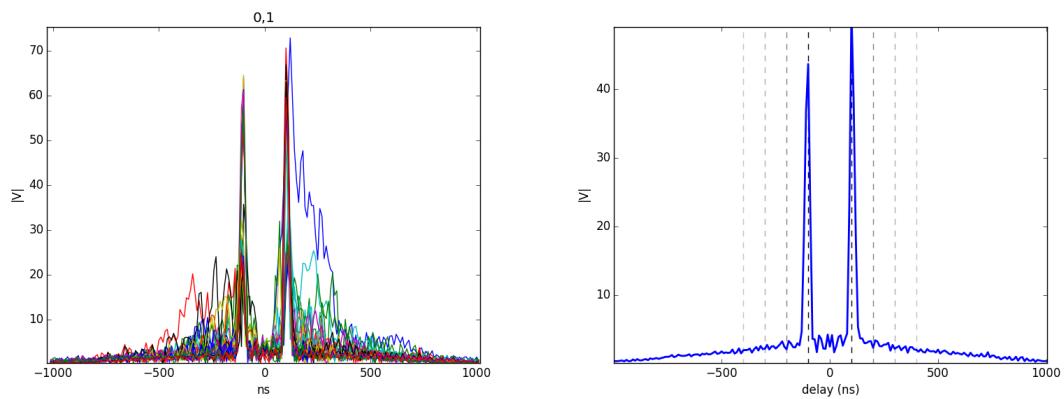


Figure 3: *Left*: The delay transform of the average signal for the night for all 30 m baselines in the array ('bad antennae' identified by OMNICAL have been removed). *Right*: The average of these signals. The dotted lines show the light-travel-time between increasing grid separations (1, 2, 3 and 4-unit separations).

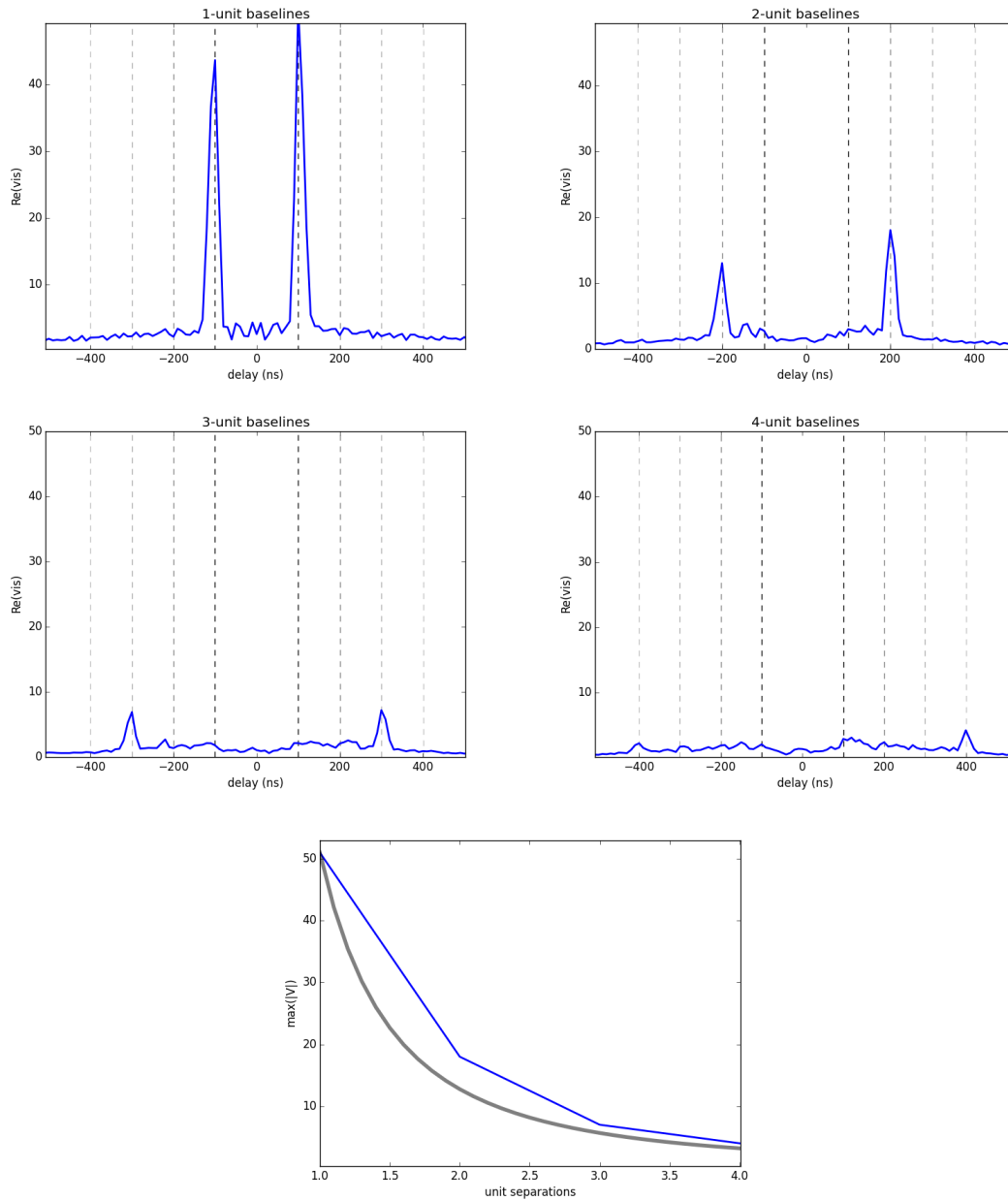


Figure 4: The average signal over the night in delay-space, averaged for baseline types of 30, 60, 90 and 120 m separations. Also shown is the relationship between the maximum value of the delay spectrum in comparison to a $1/R^2$ falloff, which it loosely follows.

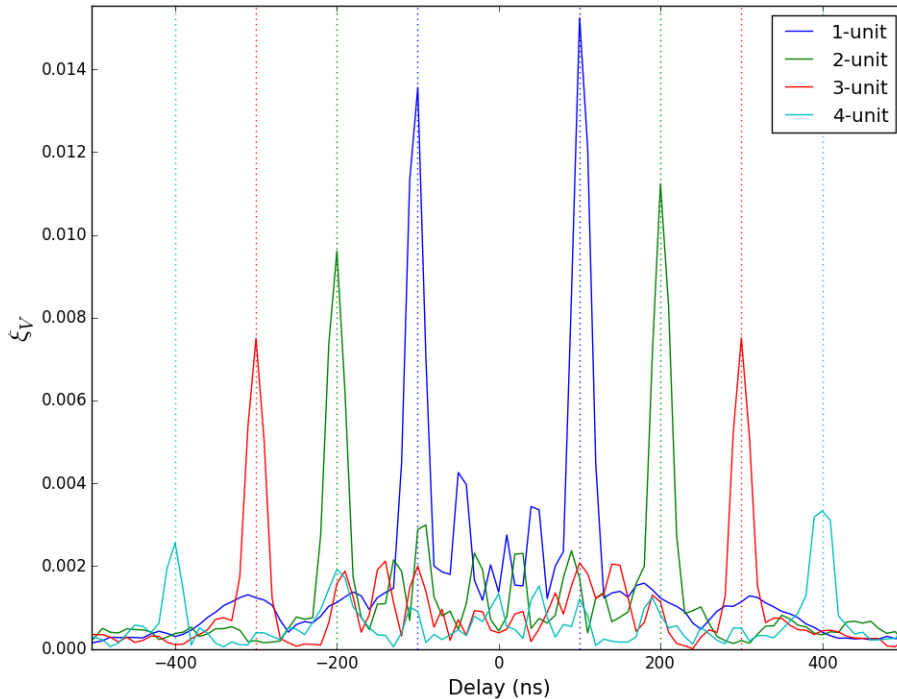


Figure 5: The value of ξ_V is a measure of how much total crosstalk is present in visibilities on average. The 30 m baselines exhibit relatively large amounts of signal ‘ringing’ outside of the horizon (shown as dotted lines for each unit-spacing).

That is, time- and baseline-averaged visibilities weighted by their RMS over frequency at each integration, should give a measure of how much crosstalk is present at each delay. This statistic is shown in Figure 5, and several interesting features are apparent. The 30 m baselines have excess power in ‘wings’, loosely corresponding to the 60 m and 90 m separations. The longer baselines may have these wings also, but at the level of noise. The noise inside the horizon on the 30 m baselines is comparable to the total crosstalk on the 120 m baselines. Note that this all occurs at levels $\sim 0.1 - 1.5\%$ of the total (foreground) signal.

4 Discussion & Conclusions

4.1 Why we care

- Crosstalk is non-astrophysical, but redundant calibration techniques such as OMNICAL [4] are ‘sky-agnostic’ and will attempt to calibrate contaminated data, leading to incorrect antenna gains and, for example, therefore risking greater $Q' \rightarrow I'$ leakage.
- Most of the crosstalk power lies outside of the horizon, especially on the shortest baselines, limiting our ability to probe the EoR window in any analysis and especially in foreground-avoidance methods such as DDR-filtering [1].
- Inaccurate crosstalk subtraction leaves artefacts in images (stripes of constant declination) which will be detrimental for imaging-based calibration such as FHD [2].
- Without any accounting for crosstalk, the XY and YX visibilities are completely overpowered by crosstalk coupled to XX and YY correlations, limiting our ability to constrain astrophysical polarization as a separate contaminant of the EoR window.

4.2 Implications for HERA

Using the formalism laid-out at the start of this memo, we hope to move forward with a common language for the collaboration to talk about crosstalk. Additions are of course welcome. We have also presented a technique for measuring crosstalk (which is being implemented for the polarized PAPER-64 power spectrum analyses and all of the PAPER-128 analyses), and shown the expected delay spectra in the presence of strong reflections.

HERA-19, now under construction in South Africa, and HERA-GB, 3 dish prototypes in Green Bank, WV, are based on design choices drawing from lessons learned from PAPER, MWA and OMNISCOPE. Different crosstalk mitigation strategies will be tested – primarily with HERA-GB – such as erecting ‘fences’ around the rim of each HERA dish. Given the points above, particular care and attention should be given to the characteristics of average visibilities in delay-space with and without crosstalk mitigation.

References

- [1] A. R. Parsons, J. C. Pober, J. E. Aguirre, C. L. Carilli, D. C. Jacobs, and D. F. Moore. A Per-baseline, Delay-spectrum Technique for Accessing the 21 cm Cosmic Reionization Signature. *ApJ*, 756:165, September 2012.
- [2] I. S. Sullivan, M. F. Morales, B. J. Hazelton, W. Arcus, D. Barnes, G. Bernardi, F. H. Briggs, J. D. Bowman, J. D. Bunton, R. J. Cappallo, B. E. Corey, A. Deshpande, L. deSouza, D. Emrich, B. M. Gaensler, R. Goeke, L. J. Greenhill, D. Herne, J. N. Hewitt, M. Johnston-Hollitt, D. L. Kaplan, J. C. Kasper, B. B. Kincaid, R. Koenig, E. Kratzenberg, C. J. Lonsdale, M. J. Lynch, S. R. McWhirter, D. A. Mitchell, E. Morgan, D. Oberoi, S. M. Ord, J. Pathikulangara, T. Prabu, R. A. Remillard, A. E. E. Rogers, A. Roshi, J. E. Salah, R. J. Sault, N. Udaya Shankar, K. S. Srivani, J. Stevens, R. Subrahmanyam, S. J. Tingay, R. B. Wayth, M. Waterson, R. L. Webster, A. R. Whitney, A. Williams, C. L. Williams, and J. S. B. Wyithe. Fast Holographic Deconvolution: A New Technique for Precision Radio Interferometry. *ApJ*, 759:17, November 2012.
- [3] A. R. Thompson, J. M. Moran, and G. W. Swenson. *Interferometry and synthesis in radio astronomy*. 1986.
- [4] H. Zheng, M. Tegmark, V. Buza, J. S. Dillon, H. Gharibyan, J. Hickish, E. Kunz, A. Liu, J. Losh, A. Lutomirski, S. Morrison, S. Narayanan, A. Perko, D. Rosner, N. Sanchez, K. Schutz, S. M. Tribiano, M. Valdez, H. Yang, K. Z. Adami, I. Zelko, K. Zheng, R. P. Armstrong, R. F. Bradley, M. R. Dexter, A. Ewall-Wice, A. Magro, M. Matejek, E. Morgan, A. R. Neben, Q. Pan, R. F. Penna, C. M. Peterson, M. Su, J. Villaseñor, C. L. Williams, and Y. Zhu. MITEoR: a scalable interferometer for precision 21 cm cosmology. *MNRAS*, 445:1084–1103, December 2014.